Renormalized cluster expansion of the microfield distribution in strongly coupled two-component plasmas

H. B. Nersisyan* and D. A. Osipyan
Division of Theoretical Physics, Institute of Radiophysics and Electronics, Alikhanian Brothers Street 1, 378410 Ashtarak, Armenia

G. Zwicknagel†
Institut für Theoretische Physik II, Erlangen-Nürnberg Universität, Staudtstrasse 7, D-91058 Erlangen, Germany
(Received 3 December 2007; published 30 May 2008)

The electric microfield distribution (MFD) at a neutral point is studied for two-component (TCP) electron-ion plasmas using molecular-dynamics simulation and theoretical models. The particles are treated within classical statistical mechanics using an electron-ion Coulomb potential regularized at distances less than the de Broglie length to take into account quantum-diffraction effects. Corrections to the potential-of-mean-force exponential (PMFEX) approximation recently proposed for the MFD at an impurity ion in a strongly coupled TCP [Nersisyan *et al.*, Phys. Rev. E **72**, 036403 (2005)] are obtained and discussed. This has been done by a generalization of the standard Baranger-Mozer and renormalized cluster expansion techniques originally developed for the one-component plasmas to the TCPs. The results from this theoretical model are compared with those from molecular-dynamics simulations. In particular, for a strongly coupled TCP with an ionic charge $Z>5$ the agreement with numerical simulations is excellent. For still increasing coupling we furthermore found that the PMFEX scheme becomes insufficient to predict the MFD at a neutral point, while its improved version quite well agrees with the simulations.

DOI: 10.1103/PhysRevE.77.056409 PACS number(s): 52.27.Gr, 52.27.Aj, 52.65.Yy, 05.10.−a

I. INTRODUCTION

The determination of the electric microfield distribution at a neutral atom or charged impurity ion (radiator) in a plasma is an important tool for the understanding of many spectroscopic experiments [1,2]. Since the pioneering work of Holtsmark [3], who completely neglected correlations between the particles (ideal plasma), many efforts have been concentrated on an improved statistical description of the microfield distribution. The first theory which goes beyond the Holtsmark limit and which is based on a cluster expansion similar to that of Ursell and Mayer [4] was developed by Baranger and Mozer [5,6]. In this approach the microfield distribution is represented as an expansion in terms of correlation functions which has been truncated on the level of the pair correlation. The latter is treated in the Debye-Hückel form which corresponds to the first order of the expansion in the coupling parameter. The theory by Baranger and Mozer was improved by Hooper [7,8]. He reformulated the expansion of the microfield distribution in terms of other functions by introducing a free parameter which was adjusted in such a way so as to arrive at a level where the resulting microfield distribution did not depend on the free parameter anymore. However, it was argued that such a method is only valid at small coupling parameters, where the correction to the Holtsmark distribution, corresponding to the first term in the series, is small. The first theory capable of providing reliable numerical results for strongly coupled plasmas, known as the adjustable-parameter exponential (APEX) approximation, was proposed by Iglesias and co-workers [9,10]. It involves a noninteracting quasiparticle representation of the electron-screened ions. This phenomenological but highly successful approximation is based on a parametrization of the electric microfield produced on a radiator with the Debye-Hückel-type screened interaction with unknown screening length. This free parameter is then adjusted in such a way to yield the correct second moment of the microfield distribution. Afterwards, the APEX model was substantially improved for neutral radiators using renormalized correlation functions and electric fields [11] (we refer the reader to Ref. [12] for a recent review).

Most of this work was done on one-component plasmas (OCPs) and thus neglects the influence of the attractive interactions between electrons and ions. This is well justified for weakly coupled plasma where the low-frequency ionic field and the high-frequency electronic field can be handled separately for spectra modeling as, e.g., considered in the early approaches [5–8]. Here the electron-ion interaction only slightly modifies these contributions. But there is an increasing number of experiments of interest which are far beyond such parameter regimes (see, e.g., Refs. [13,14]). In such cases a simple superposition of the electronic and ionic fields becomes insufficient due to strong nonlinear effects and the total field in a two-component plasmas (TCP) should serve as the starting point for spectra modeling. The related microfield distribution (MFD) including the full attractive electron-ion interaction has thus been attracting more and more attention and has already been studied, e.g., in Refs. [15–19]. In Ref. [15] the low-frequency component of the microfield was calculated within the linear response treatment taking strong correlations into account via local field corrections. In Ref. [16] the MFD in a TCP with partially degenerate electrons was investigated, while in Ref. [17] the problem of the attractive interaction was considered for a

*hrachya@irphe.am
†zwicknagel@theorie2.physik.uni-erlangen.de

single but highly charged impurity ion immersed in an electron plasma. In recent papers [18,19] we studied the MFD in a strongly coupled classical (nondegenerated) TCP beyond a perturbative treatment. In such systems the electron-ion attractive interaction drastically changes the physical properties compared to classical OCPs (see, e.g., Ref. [17]). But the thermodynamic stability of a TCP requires at least some quantum features for the electron-ion interaction at short distances, which are taken into account here by using a regularized electron-ion potential [20–22]. This enables the application of classical statistical mechanics and classical molecular-dynamics (MD) simulations as reference for theoretical treatments. As in Ref. [15], the theoretical scheme presented in Ref. [18] is based on the potential-of-mean-force exponential (PMFEX) approximation. It exactly satisfies the sum-rule requirement arising from the second moment of the microfield distribution without introducing adjustable parameters. Comparisons of the PMFEX calculations with the MD simulations for the electric fields at the highly charged points relevant for laser-produced plasmas show, in general, an excellent agreement even for large coupling [18]. First applications of the PMFEX model to the MFD at a neutral point showed, however, that this case needs further attention and improvement, similar as it occurs in the APEX scheme when considering the microfield distribution at neutral point; see Ref. [11]. In this paper we therefore focus on improvements of the description of the MFD at a neutral point in two-component plasmas. This is done by introducing the key ideas of the PMFEX approximation in the standard Baranger-Mozer cluster representation for the microfield distributions [5,6]. In this way contact between PMFEX and standard weak coupling theories is established, where the PMFEX approximation provides the leading term in a series from which corrections can be calculated explicitly.

The paper is organized as follows. In Sec. II, we define the basic parameters of interest for a TCP and the MFD in a classical canonical ensemble. In Sec. III the Baranger-Mozer treatment is reviewed for the present case of a TCP and the structure of the resulting cluster series is discussed. The basic assumptions of the PMFEX approximation are briefly given and motivated in Sec. IV. Next, a formal relationship of the PMFEX approximation to the Baranger-Mozer series is established and the first two terms of a renormalized cluster series are given explicitly. To test the proposed theoretical scheme its predictions for the MFD at a neutral point are compared with the results from classical MD simulations in Sec. V. Our findings are summarized and concluded in Sec. VI. The exact second moment of the microfield distribution at a neutral point is considered in the Appendix.

II. MICROFIELD DISTRIBUTION IN A TCP

A. Basic parameters for the TCP

We consider a neutral and isotropic two-component electron-ion plasma consisting of ions and electrons at a temperature T in a volume Ω. The particles are assumed to be classical and pointlike. The average densities, charges, and masses of the ions and electrons are n_i, n_e, and Ze, $-e$, and m_i, m, respectively. We assume that the density of radiator ions or atoms is small, $n_R \ll n_{i,e}$, and thus consider only one radiator ion with charge $Z_R e$ (or a neutral atom with $Z_R=0$) in our calculations (throughout this paper the index R refers to the radiators). Because of the charge neutrality we have $n_e=n_i Z$.

We now introduce the Coulomb coupling parameters $\Gamma_{\alpha\beta}$. Introducing the Wigner-Seitz radii—i.e., the mean electron-electron, electron-ion, and ion-ion distances—through the relations $a_e^{-3}=4\pi n_e/3$, $a^{-3}=4\pi n/3$, and $a_i^{-3}=4\pi n_i/3$ (where $n=n_e+n_i$ is the plasma total density), these parameters are defined as

$$\Gamma_{ee}=\frac{e_S^2}{a_e k_B T}, \quad \Gamma_{ei}=\frac{Ze_S^2}{a k_B T}, \quad \Gamma_{ii}=\frac{Z^2 e_S^2}{a_i k_B T}, \tag{1}$$

respectively, where $e_S^2=e^2/4\pi\varepsilon_0$. Note that

$$\Gamma_{ee}=\frac{\Gamma_{ei}}{[Z^2(Z+1)]^{1/3}}, \quad \Gamma_{ii}=\frac{Z\Gamma_{ei}}{(Z+1)^{1/3}}. \tag{2}$$

In a plasma with $Z=1$ we obtain $\Gamma_{ee}=\Gamma_{ii}=2^{-1/3}\Gamma_{ei}$, while in a plasma with highly charged ions $(Z\gg 1)$ $\Gamma_{ii}=Z^{2/3}\Gamma_{ei}\gg\Gamma_{ee}=\Gamma_{ei}/Z$. So in the TCP with uncorrelated electrons the ions may be strongly correlated.

The Holtsmark field E_H for a TCP is given by $E_H^{3/2}=E_{He}^{3/2}+E_{Hi}^{3/2}$ (see Ref. [18] for details), where E_{He} and E_{Hi} are the electronic and ionic Holtsmark fields, respectively, $E_{He}=Ce_F/a_e^2$ and $E_{Hi}=CZe_F/a_i^2$, with $C=(8\pi/25)^{1/3}$ and $e_F=e/4\pi\varepsilon_0$. Since $E_{He}=Z^{-1/3}E_{Hi}$, the electronic and ionic components of a TCP with $Z=1$ contribute equally to the Holtsmark field. For a completely ionized TCP with highly charged ions the ions dominate E_H. The definition of the Holtsmark field E_H for a TCP is equivalent to the obvious relation $n=n_e+n_i$ and can be represented as

$$E_H=\frac{C\mathcal{Z}e_F}{a^2}, \quad \mathcal{Z}=\left[\frac{Z(1+Z^{1/2})}{(Z+1)}\right]^{2/3}, \tag{3}$$

with an effective charge $\mathcal{Z}$.

For the regularized pair interaction potential $e_S^2 q_\alpha q_\beta u_{\alpha\beta}(r)$ with $\alpha,\beta=e,i,R$, $q_e=-1$, $q_i=Z$, and $q_R=Z_R$, we here employ

$$u_{\alpha\beta}(r)=\frac{1}{r}(1-e^{-r/\delta_{\alpha\beta}}). \tag{4}$$

The cutoff parameters $\delta_{\alpha\beta}$ are related to the thermal de Broglie wavelengths, $\delta_{\alpha\beta}=(\hbar^2/\mu_{\alpha\beta}k_B T)^{1/2}$, where $\mu_{\alpha\beta}$ is the reduced mass of particles α and β. For large distances $r>\delta_{\alpha\beta}$ the potential becomes Coulomb, while for $r<\delta_{\alpha\beta}$ the Coulomb singularity is removed and $u_{\alpha\beta}(0)=1/\delta_{\alpha\beta}$. By this short-range effects based on the uncertainty principle are included [20–22]. We point out that the dependence on the physical parameters density and temperature is implicitly contained in the parameters $\Gamma_{\alpha\beta}$ and $\delta_{\alpha\beta}$.

B. Microfield distribution in the canonical ensemble

The electric MFD $Q(\mathbf{E})$ is defined as the probability density of finding a field $\mathbf{E}$ at a charge $Z_R e$ or a neutral particle, located at $\mathbf{r}_0$, in a TCP with N_i ions and N_e electrons. This

system is described by classical statistical mechanics in a canonical ensemble of N_i+N_e+1 particles and temperature T. The normalized probability density of the microfield $\mathbf{E}$ is then given by [15,18]

$$Q(\mathbf{E}) = \frac{1}{W}\int_\Omega e^{-\beta_T U(\mathcal{T}_e,\mathcal{T}_i,\mathbf{r}_0)}\delta(\mathbf{E}-\mathbf{E}(\mathcal{T}_e,\mathcal{T}_i,\mathbf{r}_0))d\mathbf{r}_0 d\mathcal{T}_e d\mathcal{T}_i, \tag{5}$$

where $\beta_T=1/k_BT$, $\mathcal{T}_e=\{\mathbf{r}_1,\mathbf{r}_2,\ldots,\mathbf{r}_{N_e}\}$ and $\mathcal{T}_i=\{\mathbf{R}_1,\mathbf{R}_2,\ldots,\mathbf{R}_{N_i}\}$ are the coordinates of electrons and ions, respectively, and

$$W = \int_\Omega e^{-\beta_T U(\mathcal{T}_e,\mathcal{T}_i,\mathbf{r}_0)}d\mathbf{r}_0 d\mathcal{T}_e d\mathcal{T}_i \tag{6}$$

is the canonical partition function. $U(\mathcal{T}_e,\mathcal{T}_i,\mathbf{r}_0)$ is the potential energy of the configuration given here by

$$U(\mathcal{T}_e,\mathcal{T}_i,\mathbf{r}_0) = e_S^2\Bigg[\frac{1}{2}\sum_{\alpha,\beta,a,b} q_\alpha q_\beta u_{\alpha\beta}(|\mathbf{r}_a^{(\alpha)}-\mathbf{r}_b^{(\beta)}|) + Z_R\sum_{\alpha,a} q_\alpha u_{\alpha R}(|\mathbf{r}_0-\mathbf{r}_a^{(\alpha)}|)\Bigg] \tag{7}$$

in terms of the pair interaction potentials $u_{\alpha\beta}(r)$ and $u_{\alpha R}(r)$, where $\alpha,\beta=e,i$, $\mathbf{r}_a^{(e)}=\mathbf{r}_a$, and $\mathbf{r}_a^{(i)}=\mathbf{R}_a$. In Eq. (7) the first sum is restricted to $a\neq b$ for identical particles, $\alpha=\beta$. The total electrical field $\mathbf{E}(\mathcal{T}_e,\mathcal{T}_i,\mathbf{r}_0)$ acting on the radiator is given by the superposition of electronic and ionic single-particle fields

$$\mathbf{E}(\mathcal{T}_e,\mathcal{T}_i,\mathbf{r}_0) = -\frac{1}{Z_R e}\nabla_0 U = \sum_{a=1}^{N_e}\mathbf{E}_e(\mathbf{r}_0-\mathbf{r}_a)+\sum_{a=1}^{N_i}\mathbf{E}_i(\mathbf{r}_0-\mathbf{R}_a). \tag{8}$$

As $\mathbf{E}_\alpha(\mathbf{r})=\frac{\mathbf{r}}{r}E_\alpha(r)$, we obtain for the electronic and ionic single-particle fields $E_e(r)=e_F u'_{eR}(r)$ and $E_i(r)=-Ze_F u'_{iR}(r)$, where the prime indicates derivative with respect to r.

The spherical symmetric interaction between plasma particles and the isotropy of the system allows us to introduce the normalized microfield distribution $P(E)=4\pi E^2 Q(E)$. It can be reexpressed in terms of the Fourier transform of $Q(E)$ through

$$P(E) = \frac{2E^2}{\pi}\int_0^\infty T(\kappa)j_0(\kappa E)\kappa^2 d\kappa,$$

$$T(\kappa) = \int_0^\infty P(E)j_0(\kappa E)dE, \tag{9}$$

and

$$T(\boldsymbol{\kappa}) = \langle e^{i\boldsymbol{\kappa}\cdot\mathbf{E}}\rangle = \frac{1}{W}\int_\Omega \exp[i\boldsymbol{\kappa}\cdot\mathbf{E}(\mathcal{T}_e,\mathcal{T}_i,\mathbf{r}_0)]e^{-\beta_T U(\mathcal{T}_e,\mathcal{T}_i,\mathbf{r}_0)}d\mathbf{r}_0 d\mathcal{T}_e d\mathcal{T}_i, \tag{10}$$

where $\langle\cdots\rangle$ denotes a statistical average and $j_0(x)=\sin x/x$ is the spherical Bessel function of order zero. The coefficients of the expansion of the function $T(\kappa)$ at $\kappa\to 0$ yield the even moments of the microfield distribution,

$$T(\kappa) = 1-\frac{\kappa^2}{6}\langle E^2\rangle+\frac{\kappa^4}{120}\langle E^4\rangle-\cdots. \tag{11}$$

A similar expansion for the function $\mathcal{L}(\kappa)$ defined by $T(\kappa)=e^{-\mathcal{L}(\kappa)}$ yields

$$\mathcal{L}(\kappa) = \frac{\kappa^2}{6}\langle E^2\rangle+\frac{\kappa^4}{72}\left[\langle E^2\rangle^2-\frac{3}{5}\langle E^4\rangle\right]+\cdots. \tag{12}$$

Therefore the Fourier transform of the MFD can be interpreted as a generating function for microfield even moments. Equations (5)–(12) describe the total MFD at the position $\mathbf{r}_0$ of the radiator generated by both the statistically distributed ions and electrons of the TCP. Since we are interested in calculating the MFD, Eq. (9), in an infinite system, the statistical average of any quantity becomes translationally invariant with respect to $\mathbf{r}_0$ and the location of the test charge may be taken as the origin without loss of generality.

III. BARANGER-MOZER CLUSTER EXPANSION FOR THE TCP

In this section we generalize the Baranger-Mozer (BM) cluster expansion technique originally developed for one-component plasmas (see, e.g., Refs. [5–8]) to the classical TCPs. This method results from two transformations of Eq. (5). The first is motivated by the fact that the required average in Eq. (10) is the product of electronic and ionic single-particle functions, $e^{i\boldsymbol{\kappa}\cdot\mathbf{E}_e(\mathbf{r}_a)}$ and $e^{i\boldsymbol{\kappa}\cdot\mathbf{E}_i(\mathbf{R}_a)}$, which have a value close to one over some volume of the system. This suggests a first transformation to the set of single-particle functions

$$\chi_a^{(\alpha)}(\boldsymbol{\kappa}) = e^{i\boldsymbol{\kappa}\cdot\mathbf{E}_\alpha(\mathbf{r}_a^{(\alpha)})}-1. \tag{13}$$

Using this transformation the exponential factor in Eq. (10) becomes (for simplicity we drop the coordinate $\mathbf{r}_0$ of the radiator)

$$\exp[i\boldsymbol{\kappa}\cdot\mathbf{E}(\mathcal{T}_e,\mathcal{T}_i)] = \prod_{a=1}^{N_e}[1+\chi_a^{(e)}(\boldsymbol{\kappa})]\prod_{b=1}^{N_i}[1+\chi_b^{(i)}(\boldsymbol{\kappa})]. \tag{14}$$

The introduced single-particle functions $\chi_a^{(\alpha)}$ have the advantage to be zero over some volume. The spirit of this transformation to the functions $\chi_a^{(\alpha)}$ is similar to the use of Mayer's f functions for thermodynamic properties of gases [4]. Substituting Eq. (14) into Eq. (10) leads in the thermodynamic limit directly to the series

$$T(\boldsymbol{\kappa}) = 1+\sum_\alpha\sum_{a=1}^\infty\frac{n_\alpha^a}{a!}\int\chi_1^{(\alpha)}(\boldsymbol{\kappa})\chi_2^{(\alpha)}(\boldsymbol{\kappa})\cdots\chi_a^{(\alpha)}(\boldsymbol{\kappa}) \times\mathcal{G}_a^{(\alpha)}(\mathcal{T}_a^{(\alpha)})d\mathcal{T}_a^{(\alpha)}+\sum_{a=1}^\infty\frac{n_e^a}{a!}\sum_{b=1}^\infty\frac{n_i^b}{b!}\int\chi_1^{(e)}(\boldsymbol{\kappa})\cdots\chi_a^{(e)}(\boldsymbol{\kappa}) \times\chi_1^{(i)}(\boldsymbol{\kappa})\cdots\chi_b^{(i)}(\boldsymbol{\kappa})\mathcal{G}_{ab}^{(ei)}(\mathcal{T}_a^{(e)},\mathcal{T}_b^{(i)})d\mathcal{T}_a^{(e)}d\mathcal{T}_b^{(i)}, \tag{15}$$

where $\mathcal{T}_a^{(\alpha)}=\{\mathbf{r}_1^{(\alpha)},\mathbf{r}_2^{(\alpha)},\ldots,\mathbf{r}_a^{(\alpha)}\}$ and $d\mathcal{T}_a^{(\alpha)}=d\mathbf{r}_1^{(\alpha)}d\mathbf{r}_2^{(\alpha)}\cdots d\mathbf{r}_a^{(\alpha)}$.

Here $\mathcal{G}_a^{(\alpha)}(\mathcal{T}_a^{(\alpha)})$ and $\mathcal{G}_{ab}^{(ei)}(\mathcal{T}_a^{(e)},\mathcal{T}_b^{(i)})$ are equilibrium correlation functions. The first quantity represents the probability density for a particles from plasma species α at $\mathbf{r}_1^{(\alpha)},\mathbf{r}_2^{(\alpha)},\ldots,\mathbf{r}_a^{(\alpha)}$ and the test particle at the origin. The second one describes the correlations between a electrons at $\mathbf{r}_1,\mathbf{r}_2,\ldots,\mathbf{r}_a$ and b ions at $\mathbf{R}_1,\mathbf{R}_2,\ldots,\mathbf{R}_b$ involving the test particle. The range of integration for each term in Eq. (15) is now restricted by the $\chi_a^{(\alpha)}(\boldsymbol{\kappa})$ functions. However, this restriction is not uniform with respect to $\boldsymbol{\kappa}$, and particularly for large values of $\boldsymbol{\kappa}$ the functions $\chi_a^{(\alpha)}(\boldsymbol{\kappa})$ can differ from zero over a correspondingly large volume. Consequently, a second transformation is desirable, $T(\boldsymbol{\kappa})=e^{-\mathcal{L}(\boldsymbol{\kappa})}$, whereby a standard theorem of equilibrium statistical mechanics (see, e.g., Ref. [23]), $\mathcal{L}(\boldsymbol{\kappa})$, is determined from Eq. (15) as

$$\mathcal{L}(\boldsymbol{\kappa}) = -\sum_{\alpha}\sum_{a=1}^{\infty}\frac{n_\alpha^a}{a!}h_a^{(\alpha)}(\boldsymbol{\kappa}) - \sum_{a=1}^{\infty}\frac{n_e^a}{a!}\sum_{b=1}^{\infty}\frac{n_i^b}{b!}h_{ab}^{(ei)}(\boldsymbol{\kappa}). \quad (16)$$

Here $h_a^{(\alpha)}(\boldsymbol{\kappa})$ and $h_{ab}^{(ei)}(\boldsymbol{\kappa})$ are given by

$$h_a^{(\alpha)}(\boldsymbol{\kappa}) = \int \chi_1^{(\alpha)}(\boldsymbol{\kappa})\chi_2^{(\alpha)}(\boldsymbol{\kappa})\cdots\chi_a^{(\alpha)}(\boldsymbol{\kappa})\ell_a^{(\alpha)}(\mathcal{T}_a^{(\alpha)})d\mathcal{T}_a^{(\alpha)}, \quad (17)$$

$$h_{ab}^{(ei)}(\boldsymbol{\kappa}) = \int \chi_1^{(e)}(\boldsymbol{\kappa})\cdots\chi_a^{(e)}(\boldsymbol{\kappa})\chi_1^{(i)}(\boldsymbol{\kappa})\cdots\chi_b^{(i)}(\boldsymbol{\kappa}) \times \ell_{ab}^{(ei)}(\mathcal{T}_a^{(e)},\mathcal{T}_b^{(i)})d\mathcal{T}_a^{(e)}d\mathcal{T}_b^{(i)}, \quad (18)$$

and $\ell_a^{(\alpha)}$ and $\ell_{ab}^{(ei)}$ are the Ursell cluster functions for TCP associated with the set of the usual correlation functions $\mathcal{G}_a^{(\alpha)}$ and $\mathcal{G}_{ab}^{(ei)}$, respectively. The functions $\ell_a^{(\alpha)}$ for electron-electron and ion-ion interactions are expressed by the correlation functions $\mathcal{G}_a^{(\alpha)}$ in the same manner as in the case of corresponding OCP (see, e.g., Refs. [5–7]). Therefore, as an example we consider here explicitly only the functions $\ell_{ab}^{(ei)}$ which involve electron-ion interactions:

$$\ell_{11}^{(ei)}(\mathbf{r}_1,\mathbf{R}_1) = \mathcal{G}_{11}^{(ei)}(\mathbf{r}_1,\mathbf{R}_1) - \mathcal{G}_1^{(e)}(\mathbf{r}_1)\mathcal{G}_1^{(i)}(\mathbf{R}_1), \quad (19)$$

$$\ell_{12}^{(ei)}(\mathbf{r}_1,\mathbf{R}_1,\mathbf{R}_2) = \mathcal{G}_{12}^{(ei)}(\mathbf{r}_1,\mathbf{R}_1,\mathbf{R}_2) - \mathcal{G}_1^{(e)}(\mathbf{r}_1)\mathcal{G}_2^{(i)}(\mathbf{R}_1,\mathbf{R}_2) - \mathcal{G}_1^{(i)}(\mathbf{R}_1)\mathcal{G}_{11}^{(ei)}(\mathbf{r}_1,\mathbf{R}_2) - \mathcal{G}_1^{(i)}(\mathbf{R}_2)\mathcal{G}_{11}^{(ei)}(\mathbf{r}_1,\mathbf{R}_1) + 2\mathcal{G}_1^{(e)}(\mathbf{r}_1)\mathcal{G}_1^{(i)}(\mathbf{R}_1)\mathcal{G}_1^{(i)}(\mathbf{R}_2), \quad (20)$$

$$\ell_{21}^{(ei)}(\mathbf{r}_1,\mathbf{r}_2,\mathbf{R}_1) = \mathcal{G}_{21}^{(ei)}(\mathbf{r}_1,\mathbf{r}_2,\mathbf{R}_1) - \mathcal{G}_1^{(i)}(\mathbf{R}_1)\mathcal{G}_2^{(e)}(\mathbf{r}_1,\mathbf{r}_2) - \mathcal{G}_1^{(e)}(\mathbf{r}_1)\mathcal{G}_{11}^{(ei)}(\mathbf{r}_2,\mathbf{R}_1) - \mathcal{G}_1^{(e)}(\mathbf{r}_2)\mathcal{G}_{11}^{(ei)}(\mathbf{r}_1,\mathbf{R}_1) + 2\mathcal{G}_1^{(e)}(\mathbf{r}_1)\mathcal{G}_1^{(e)}(\mathbf{r}_2)\mathcal{G}_1^{(i)}(\mathbf{R}_1), \quad (21)$$

etc., for pair and three-body correlations, respectively. The higher-order Ursell functions involving ≥ 4 particles can be constructed similarly. All single-particle Ursell functions are here expressed by the ordinary pair correlation function between radiator and plasma particles of species α, $\ell_1^{(\alpha)}(\mathbf{r}) = \mathcal{G}_1^{(\alpha)}(\mathbf{r}) = g_{\alpha R}(r)$ [18]. The significant difference between $\mathcal{G}$ and ℓ correlation functions is that the cluster functions ℓ vanish when any members of the particles are sufficiently far apart, whereas the ordinary correlation functions $\mathcal{G}$ do not have this property. In particular, for completely uncorrelated systems of particles the many-body functions $\mathcal{G}$ tend to unity while $\ell \to 0$ beginning with $\ell_{11}^{(ei)}$ and $\ell_2^{(\alpha)}$. Hence, the range of integrals in Eq. (16) is controlled by both the functions $\chi_a^{(\alpha)}(\boldsymbol{\kappa})$ and the Ursell functions. The latter restricts the integration to volumes characterized by the correlation length, which depends on the thermodynamic-state condition, but is independent of $\boldsymbol{\kappa}$. Qualitatively, therefore, the BM formalism provides a series representation whose terms are controlled by the range of $\chi_a^{(\alpha)}(\boldsymbol{\kappa})$ for small $\boldsymbol{\kappa}$ and by the range of the Ursell functions for large $\boldsymbol{\kappa}$.

Equations (16)–(18) together with the relation $T(\boldsymbol{\kappa}) = e^{-\mathcal{L}(\boldsymbol{\kappa})}$ constitutes the generalization of the Baranger-Mozer cluster expansion technique to the TCPs. In contrast to the BM theory developed for OCPs, Eq. (16) now involves terms which are responsible for electron-electron, ion-ion, and electron-ion attractive interactions. The BM result is easily recovered from Eq. (16) by neglecting the last term as well as one of two terms responsible for the interactions between identical particles. In addition, for ideal TCPs (Holtsmark limit) the second sum in Eq. (16) and all terms with $a \geq 2$ in the first sum vanish, and only the term with $a=1$ in the first sum contributes to the MFD. It is easy to see that this term coincides with the result of Ref. [18] derived for ideal TCPs.

From a practical point of view, it is too difficult to calculate correlation functions of higher order than $\mathcal{G}_2^{(\alpha)}$ and $\mathcal{G}_{11}^{(ei)}$. For weakly coupled plasmas, the Ursell functions of order $\lambda+1$ are typically of the order of the plasma parameters to the power λ. Therefore Eq. (16) is usually truncated at first, second, or in some cases third order. If the correlation functions are expanded as well with respect to the plasma parameters and truncated at the corresponding order, the MFD with Eqs. (16)–(18) can be evaluated analytically (see, e.g., Refs. [5–8,24,25]). Obviously, such a method may be successful only for weakly coupled plasmas. A possible extension to the strongly coupled regimes requires that the BM representation sufficiently rapidly converge to allow for a truncation after the first two terms. This suggests, for instance, that the BM series could be improved if the bare single-particle electric fields in the χ functions are replaced by screened fields representing the effects of strong correlations in a plasma. The formal procedure for carrying out such a "renormalization" has been developed in Ref. [26] and has been previously employed for OCPs [11]. In the next Sec. IV we extend this renormalization procedure to the two-component plasmas.

IV. RENORMALIZATION OF THE BARANGER-MOZER CLUSTER SERIES

A. PMFEX approximation as independent-particle model

The predictions of APEX approximation for the MFD show excellent agreement with numerical simulation data for OCPs. However, difficulties appear when one attempts to extend the APEX scheme to a TCP, e.g., by assuming a Debye-Hückel-type interaction separately for the electrons and the ions and introducing two adjustable screening lengths. Then the second moment sum rule becomes ambiguous [see, e.g., Eq. (29) below] as it allows for many different choices of the adjustable screening lengths. This can be

cured for ionic mixtures by demanding that the second moment rule be satisfied species by species (see, e.g., Ref. [27]). But this cannot be employed for a TCP with attractive electron-ion interactions. Here the Debye-Hückel ansatz for the electronic effective field is physically incompatible with the second moment requirement as discussed in Ref. [15].

In Refs. [18,19] we instead introduced the PMFEX approximation which links the MFD to the pair correlation functions. To make further progress we briefly outline here the basic concepts of the PMFEX approximation. We show that similarly to the APEX approximation (see, e.g., Ref. [9–11]) the PMFEX approximation is also an effective independent-particle model. Based on this assumption the MFD within PMFEX approximation is derived quite simply. If all interactions between the plasma particles, except those with the radiator, are neglected, then the Ursell functions $\ell_a^{(\alpha)}$ vanish for $a \geq 2$ and $\ell_{ab}^{(ei)}(\mathcal{T}_a^{(e)}, \mathcal{T}_b^{(i)}) = 0$ for arbitrary a and b. The BM series (16) then reduces to only the leading term

$$\mathcal{L}^{(0)}(\boldsymbol{\kappa}) = -\sum_\alpha n_\alpha \int \chi_1^{(\alpha)}(\boldsymbol{\kappa}) g_{\alpha R}^{(0)}(\mathbf{r}_1) d\mathbf{r}_1 . \tag{22}$$

The superscript (0) denotes the corresponding quantity without interactions among plasma particles. The PMFEX approach retains the independent-particle form of (22),

$$\mathcal{L}^{(0)}(\boldsymbol{\kappa}) \to \mathcal{L}(\boldsymbol{\kappa}) = -\sum_\alpha n_\alpha \int \psi_1^{(\alpha)}(\boldsymbol{\kappa}) g_{\alpha R}^{*}(\mathbf{r}_1) d\mathbf{r}_1 , \tag{23}$$

with the assumption that the important effects of correlations can be accounted for by an effective pair distribution function $g_{\alpha R}^{*}(\mathbf{r}_1)$ and a screened field $\mathcal{E}_\alpha(\mathbf{r}_1)$ replacing the single-particle field $\mathbf{E}_\alpha(\mathbf{r}_1)$ in $\chi_1^{(\alpha)}(\boldsymbol{\kappa})$:

$$\psi_1^{(\alpha)}(\boldsymbol{\kappa}) = e^{i\boldsymbol{\kappa}\cdot\mathcal{E}_\alpha(\mathbf{r}_1)} - 1 . \tag{24}$$

Some constraint must be imposed to determine $g_{\alpha R}^{*}(\mathbf{r}_1)$. As in the case of the APEX approximation [9], this is a requirement that the effective "quasiparticle" field due to the effective charge density at $\mathbf{r}_1$ be equal to the corresponding exact field:

$$g_{\alpha R}^{*}(\mathbf{r}_1)\mathcal{E}_\alpha(\mathbf{r}_1) = g_{\alpha R}(\mathbf{r}_1)\mathbf{E}_\alpha(\mathbf{r}_1) . \tag{25}$$

Assuming spherical symmetric interactions with $\mathcal{E}_\alpha(\mathbf{r}) = \frac{\mathbf{r}}{r}\mathcal{E}_\alpha(r)$ and $\mathbf{E}_\alpha(\mathbf{r}) = \frac{\mathbf{r}}{r}E_\alpha(r)$, this condition then defines the PMFEX model as

$$\mathcal{L}_{\mathrm{PMFEX}}(\kappa) = \sum_\alpha 4\pi n_\alpha \int_0^\infty E_\alpha(r) \frac{1 - j_0(\kappa\mathcal{E}_\alpha(r))}{\mathcal{E}_\alpha(r)} g_{\alpha R}(r) r^2 dr . \tag{26}$$

In practice, $g_{\alpha R}(r)$ is calculated from the hypernetted-chain (HNC) integral equation [28,29] extended to the TCP (see, e.g., Refs. [18,19]).

In the APEX model originally developed for classical ionic OCPs with bare Coulomb interactions to determine the effective field, a second requirement is needed. In Ref. [9] the effective field $\mathcal{E}(r)$ is assumed as a Debye-Hückel-type screened interaction with unknown screening length. This free parameter is then adjusted in such a way so as to satisfy the exact second-moment requirement. In contrast to the APEX method the effective fields $\mathcal{E}_\alpha(r)$ in the PMFEX model are obtained automatically (see Ref. [18] for details), employing thermodynamic perturbation theory [30]. We recall here these effective fields for completeness. For simplicity, assuming a Coulomb potential for the repulsive interactions—i.e., $\delta_{ee} = \delta_{ii} = 0$ (electron-electron and ion-ion interactions)—and regularized one [see Eq. (4)] for electron-ion interactions these fields read [18]

$$\mathcal{E}_\alpha(r) = E_\alpha(r)\left\{1 + \frac{4\pi n_\alpha}{g_{\alpha R}(r)} \int_0^r [g_{\alpha\alpha}(\rho) - g_{ei}(\rho)]\rho^2 d\rho \right\}, \tag{27}$$

where $E_\alpha(r) = q_\alpha e_F / r^2$ are the bare single-particle fields. Based on the derivations given in Ref. [18] it is straightforward to show that the effective fields $\mathcal{E}_\alpha(r)$ can be alternatively represented as the logarithmic derivative of the radial distribution functions (RDFs) $g_{\alpha R}(r)$ as

$$\mathcal{E}_\alpha(r) = \frac{k_B T}{Z_R e} \frac{\partial}{\partial r} [\ln g_{\alpha R}(r)], \tag{28}$$

which is known as the potential-of-mean-force (PMF) approximation proposed by Yan and Ichimaru [15] (see also Ref. [28]).

Using Eq. (12) we expand Eq. (26) around a value $\kappa = 0$ and find the second moment of the MFD in the PMFEX model:

$$\langle E^2 \rangle_{\mathrm{PMFEX}} = \sum_\alpha 4\pi n_\alpha \int_0^\infty \mathcal{E}_\alpha(r) E_\alpha(r) g_{\alpha R}(r) r^2 dr . \tag{29}$$

Introducing now Eq. (28), which is valid for a charged radiator with $Z_R \neq 0$, in Eq. (29) automatically satisfies the exact sum rule $\langle E^2 \rangle_{\mathrm{PMFEX}} = \langle E^2 \rangle$ without any adjustable parameter. Here $\langle E^2 \rangle$ is the exact second moment of the MFD as derived in Ref. [18] for the TCP; see also Eq. (A1). Thus, if the $g_{\alpha R}(r)$ are known, the MFD can be calculated using Eqs. (9), (26), and (28). For the MFD at a charged radiator, taking the required $g_{\alpha R}$ from corresponding HNC calculations, the PMFEX scheme has been tested by comparison with results of MD simulations. Both the $g_{\alpha R}$ from the HNC and the MFD from the PMFEX approximation are in general in excellent agreement with the MD simulation, with some deviations in a regime dominated by small local fields and hence by small local electronic density.

In the case of a neutral radiator—i.e., in the limit $Z_R \to 0$, in which we are interested here—the PMF ansatz (28) is not applicable as the RDFs tend to unity, $g_{\alpha R} \to 1$ and $\ln g_{\alpha R}(r) \to 0$. But based on the derivations given in Refs. [18] (see also the Appendix for details), the correct limit $Z_R \to 0$ can be done and results in the effective field of Eq. (27) when setting $g_{\alpha R}(r) = 1$. Calculating now Eq. (27) again with $g_{\alpha\beta}$ taken from HNC and subsequently the MFD via Eqs. (9) and (26) yields, however, a less satisfactory agreement with the simulation than in the case of a charged point. This was the major motivation to reformulate the theoretical scheme in terms of a renormalized cluster series which will be outlined in the next section.

B. Renormalized cluster series

The comments at the end of Sec. III and the success of the PMFEX approximation indicate that the Baranger-Mozer series could be improved if the single-particle field in the functions $\chi_a^{(\alpha)}(\boldsymbol{\kappa})$ is replaced by a screened field representing the effects of correlations in strongly coupled plasmas. In this spirit, a new functional series is obtained in terms of the renormalized functions $\psi_a^{(\alpha)}(\boldsymbol{\kappa})$ of Eq. (24) by the definition $\mathcal{L}^*[\psi_a;\boldsymbol{\kappa}]=\mathcal{L}[\chi_a;\boldsymbol{\kappa}]$, which is easily obtained from the BM series Eqs. (16)–(18) and the functional relationship between $\chi_a^{(\alpha)}$ and $\psi_a^{(\alpha)}$. Introducing the functions $\mathcal{R}_\alpha(r)$ by the relation $\mathcal{E}_\alpha(r)=\mathcal{R}_\alpha(r)E_\alpha(r)$ (we assume spherical symmetric interactions) with the effective $\mathcal{E}_\alpha(r)$ and single-particle $E_\alpha(r)$ fields, the functional relation between $\chi_a^{(\alpha)}$ and $\psi_a^{(\alpha)}$ is established as

$$\chi_a^{(\alpha)}(\boldsymbol{\kappa})=[1+\psi_a^{(\alpha)}(\boldsymbol{\kappa})]^{1/\mathcal{R}_\alpha(r_a)}-1. \tag{30}$$

To obtain the new function $\mathcal{L}^*[\psi_a;\boldsymbol{\kappa}]$, which must be multilinear with respect to ψ_a [cf. Eqs. (16)–(18)], we expand the $\chi_a^{(\alpha)}$-functions in Eq. (30) with respect to the $\psi_a^{(\alpha)}$ functions [31]:

$$\begin{aligned}\chi_a^{(\alpha)}(\boldsymbol{\kappa})=&\frac{\psi_a^{(\alpha)}(\boldsymbol{\kappa})}{\mathcal{R}_\alpha(r_a)}+\frac{[\psi_a^{(\alpha)}(\boldsymbol{\kappa})]^2}{2!}\frac{1}{\mathcal{R}_\alpha(r_a)}\left[\frac{1}{\mathcal{R}_\alpha(r_a)}-1\right]\\&+\frac{[\psi_a^{(\alpha)}(\boldsymbol{\kappa})]^3}{3!}\frac{1}{\mathcal{R}_\alpha(r_a)}\left[\frac{1}{\mathcal{R}_\alpha(r_a)}-1\right]\left[\frac{1}{\mathcal{R}_\alpha(r_a)}-2\right]\\&+\cdots.\end{aligned} \tag{31}$$

Then elimination of $\chi_a^{(\alpha)}$ on the right-hand side of the equation $\mathcal{L}^*[\psi_a;\boldsymbol{\kappa}]=\mathcal{L}[\chi_a;\boldsymbol{\kappa}]$ using Eq. (31) yields the desired renormalized cluster series

$$\mathcal{L}^*[\psi_a;\boldsymbol{\kappa}]=-\sum_\alpha\sum_{a=1}^{\infty}\frac{n_\alpha^a}{a!}H_a^{(\alpha)}(\boldsymbol{\kappa})-\sum_{a=1}^{\infty}\frac{n_e^a}{a!}\sum_{b=1}^{\infty}\frac{n_i^b}{b!}H_{ab}^{(ei)}(\boldsymbol{\kappa}). \tag{32}$$

Here

$$H_a^{(\alpha)}(\boldsymbol{\kappa})=\int\psi_1^{(\alpha)}(\boldsymbol{\kappa})\psi_2^{(\alpha)}(\boldsymbol{\kappa})\cdots\psi_a^{(\alpha)}(\boldsymbol{\kappa})L_a^{(\alpha)}(\mathcal{T}_a^{(\alpha)})d\mathcal{T}_a^{(\alpha)}, \tag{33}$$

$$\begin{aligned}H_{ab}^{(ei)}(\boldsymbol{\kappa})=&\int\psi_1^{(e)}(\boldsymbol{\kappa})\psi_2^{(e)}(\boldsymbol{\kappa})\cdots\psi_a^{(e)}(\boldsymbol{\kappa})\psi_1^{(i)}(\boldsymbol{\kappa})\psi_2^{(i)}(\boldsymbol{\kappa})\cdots\\&\times\psi_b^{(i)}(\boldsymbol{\kappa})L_{ab}^{(ei)}(\mathcal{T}_a^{(e)},\mathcal{T}_b^{(i)})d\mathcal{T}_a^{(e)}d\mathcal{T}_b^{(i)},\end{aligned} \tag{34}$$

with the generalized Ursell functions $L_a^{(\alpha)}$ and $L_{ab}^{(ei)}$, which are recognized as the functional derivatives of $H_a^{(\alpha)}(\boldsymbol{\kappa})$ and $H_{ab}^{(ei)}(\boldsymbol{\kappa})$, respectively. Explicitly the first- and second-order generalized Ursell functions are found to be

$$L_1^{(\alpha)}(r_1)=\frac{g_{\alpha R}(r_1)}{\mathcal{R}_\alpha(r_1)}, \tag{35}$$

$$\begin{aligned}L_2^{(\alpha)}(\mathbf{r}_1,\mathbf{r}_2)=&\frac{g_{\alpha\alpha}(|\mathbf{r}_1-\mathbf{r}_2|)-g_{\alpha R}(r_1)g_{\alpha R}(r_2)}{\mathcal{R}_\alpha(r_1)\mathcal{R}_\alpha(r_2)}\\&-\frac{1}{n_\alpha}\delta(\mathbf{r}_1-\mathbf{r}_2)g_{\alpha R}(r_1)\frac{\mathcal{R}_\alpha(r_1)-1}{\mathcal{R}_\alpha^2(r_1)},\end{aligned} \tag{36}$$

$$L_{11}^{(ei)}(\mathbf{r}_1,\mathbf{R}_1)=\frac{g_{ei}(|\mathbf{r}_1-\mathbf{R}_1|)-g_{eR}(r_1)g_{iR}(R_1)}{\mathcal{R}_e(r_1)\mathcal{R}_i(R_1)}, \tag{37}$$

which result in the first three terms in Eq. (32):

$$\begin{aligned}\mathcal{L}^*(\boldsymbol{\kappa})=\mathcal{L}(\boldsymbol{\kappa})=&-\sum_\alpha n_\alpha\int\frac{\psi_1^{(\alpha)}(\boldsymbol{\kappa})}{\mathcal{R}_\alpha(r)}g_{\alpha R}(r)d\mathbf{r}\\&-\sum_\alpha\frac{n_\alpha^2}{2}\left\{\int\frac{\psi_1^{(\alpha)}(\boldsymbol{\kappa})\psi_2^{(\alpha)}(\boldsymbol{\kappa})}{\mathcal{R}_\alpha(r_1)\mathcal{R}_\alpha(r_2)}[g_{\alpha\alpha}(|\mathbf{r}_1-\mathbf{r}_2|)\right.\\&-g_{\alpha R}(r_1)g_{\alpha R}(r_2)]d\mathbf{r}_1d\mathbf{r}_2+\frac{1}{n_\alpha}\int[\psi_1^{(\alpha)}(\boldsymbol{\kappa})]^2\\&\left.\times\frac{1-\mathcal{R}_\alpha(r_1)}{\mathcal{R}_\alpha^2(r_1)}g_{\alpha R}(r_1)d\mathbf{r}_1\right\}\\&-n_en_i\int\frac{\psi_1^{(e)}(\boldsymbol{\kappa})\psi_1^{(i)}(\boldsymbol{\kappa})}{\mathcal{R}_e(r_1)\mathcal{R}_i(R_1)}[g_{ei}(|\mathbf{r}_1-\mathbf{R}_1|)\\&-g_{eR}(r_1)g_{iR}(R_1)]d\mathbf{r}_1d\mathbf{R}_1.\end{aligned} \tag{38}$$

The first term of Eq. (38) is seen to be precisely the PMFEX approximation [cf. Eqs. (23) and (25)]. The factor of $\mathcal{R}_\alpha(r)$ occurs automatically here from the renormalization and eliminates the assumption (25) of the PMFEX approximation.

Finally the angular integration in Eq. (38) can be performed using spherical harmonic expansion [31]. This yields

$$\mathcal{L}(\kappa)=\mathcal{L}_{\mathrm{PMFEX}}(\kappa)+\Delta\mathcal{L}(\kappa), \tag{39}$$

where the first term is the PMFEX result, Eq. (26), and the second term represents the corrections due to the renormalization:

$$\begin{aligned}\Delta\mathcal{L}(\kappa)=&2\pi\sum_\alpha n_\alpha\int_0^\infty[j_0(2\kappa\mathcal{E}_\alpha(r))-2j_0(\kappa\mathcal{E}_\alpha(r))+1]\\&\times\frac{\mathcal{R}_\alpha(r)-1}{\mathcal{R}_\alpha^2(r)}g_{\alpha R}(r)r^2dr-4\sum_\alpha n_\alpha\int_0^\infty G_{\alpha\alpha}(\kappa,k)\\&\times[S_{\alpha\alpha}(k)-1]k^2dk-8\frac{n_en_i}{n}\int_0^\infty G_{ei}(\kappa,k)S_{ei}(k)k^2dk\\&+\frac{1}{2}[\mathcal{L}_{\mathrm{PMFEX}}^2(\kappa)-\mathcal{L}_0^2(\kappa)].\end{aligned} \tag{40}$$

Here $\mathcal{L}_0(\kappa)$ is the $\mathcal{L}_{\mathrm{PMFEX}}(\kappa)$ given by Eq. (26), but with $g_{\alpha R}(r)=1$:

$$\mathcal{L}_0(\kappa)=\sum_\alpha 4\pi n_\alpha\int_0^\infty\frac{1-j_0(\kappa\mathcal{E}_\alpha(r))}{\mathcal{R}_\alpha(r)}r^2dr. \tag{41}$$

In Eq. (40) the term $S_{\alpha\beta}(k)$ (with $\alpha,\beta=e,i$) is the static structure factor for the two-component plasma,

$$S_{\alpha\beta}(k) = \delta_{\alpha\beta} + 4\pi n_{\alpha\beta}\int_0^\infty [g_{\alpha\beta}(r) - 1]j_0(kr)r^2 dr, \quad (42)$$

with $\delta_{\alpha\alpha}=1$, $\delta_{ei}=0$, $n_{\alpha\alpha}=n_\alpha$, and $n_{ei}=n=n_e+n_i$, and $G_{\alpha\beta}(\kappa,k)$ is defined by

$$G_{\alpha\beta}(\kappa,k) = \sum_{l=0}^{\infty}(-1)^l(2l+1)J_l^{(\alpha)}(\kappa,k)J_l^{(\beta)}(\kappa,k), \quad (43)$$

$$J_l^{(\alpha)}(\kappa,k) = \int_0^\infty j_l(kr)[j_l(\kappa\mathcal{E}_\alpha(r)) - \delta_{l0}]\frac{r^2 dr}{\mathcal{R}_\alpha(r)}. \quad (44)$$

Also, $j_l(x)$ is the spherical Bessel function of order l. It should be noted that for deriving the renormalized series Eq. (32) we do not use the explicit functional form of $\mathcal{E}_\alpha(r)$. Hence, in spite of its important role in the theory, the precise functional form of the effective field $\mathcal{E}_\alpha(r)$ may remain arbitrary. Moreover, it is straightforward to show that the generating function (16) as well as its renormalized version (32) yields exact even moments of the MFD according to Eq. (12) independently of the functional form of $\mathcal{E}_\alpha(r)$. In the present context it might appear more reasonable to choose $\mathcal{E}_\alpha(r)$ to improve convergence of the renormalized series (32). A similar procedure is used in thermodynamic perturbation theory where the corresponding parameters of the leading term are chosen to make the next order terms vanish [32]. But this is not possible without making $\mathcal{E}_\alpha(r)$ a function of κ (see similar discussion in Ref. [11] in the context of the APEX approximation). Here we consider for $\mathcal{E}_\alpha(r)$ the mean-force field as derived in Ref. [18] for the TCP [see also Eq. (28) as well as Eq. (27) for the repulsive Coulomb interactions] and which appears automatically from the second-moment condition $\partial^2\mathcal{L}^*/\partial\kappa^2|_{\kappa=0}=\frac{1}{3}\langle E^2\rangle$ for the renormalized function $\mathcal{L}^*$, Eq. (32). The theoretical scheme resulting from Eqs. (39)–(44) is abbreviated as PMFEX+. It agrees for neutral points quite well with the MD simulation results, as we will show in the next section. It is straightforward to show that the correction $\Delta\mathcal{L}(\kappa)$ in Eq. (39) behaves as $\sim\kappa^4$ at $\kappa\to 0$ and, therefore, does not contribute to the second moment. Then the quantity $\langle E^2\rangle$ receives a contribution only from the PMFEX term in Eq. (39).

V. MFD AT A NEUTRAL RADIATOR

In the case of a neutral radiator, $Z_R=0$, the plasma-radiator correlation functions are $g_{\alpha R}(r)=1$ and Eq. (40) is simplified. In particular, the last term vanishes since $\mathcal{L}_{\mathrm{PMFEX}}(\kappa)=\mathcal{L}_0(\kappa)$ for $g_{\alpha R}(r)=1$. Thus, the generating function $\mathcal{L}(\kappa)$ of the MFD in the PMFEX+ model is given by $\mathcal{L}(\kappa)=\mathcal{L}_0(\kappa)+\Delta\mathcal{L}(\kappa)$, where $\mathcal{L}_0(\kappa)$ is the ordinary PMFEX expression, with $g_{\alpha R}(r)=1$; see Eq. (41). The higher-order corrections are involved in the second term $\Delta\mathcal{L}(\kappa)$. The functions $\mathcal{R}_\alpha(r)$ are obtained from Eq. (27),

$$\mathcal{R}_\alpha(r) = 1 + 4\pi n_\alpha\int_0^r [g_{\alpha\alpha}(\rho) - g_{ei}(\rho)]\rho^2 d\rho, \quad (45)$$

which in the limit of small plasma-parameters ($\Gamma_{ee}\to 0$) can be evaluated explicitly using the Debye-Hückel approximation $\mathcal{R}_e(r)=\mathcal{R}_i(r)\simeq(\frac{r}{\lambda}+1)e^{-r/\lambda}$. Here $\lambda^2=\varepsilon_0 k_B T/(Zne^2)$ is the Debye screening length. Thus, similar to the standard PMFEX, the PMFEX+ approximation links the MFD to the RDFs. To obtain explicit results for the MFD the corresponding RDFs and the static structure factors must be determined first. This is done by solving numerically the HNC integral equations [28,29] for the TCPs under consideration (see Ref. [18] and references therein for more details). For simplicity we assume here bare Coulomb interactions for electron-electron and ion-ion interactions—i.e., $\delta_{ee}\simeq 0$ and $\delta_{ii}\simeq 0$—and a regularized electron-ion interaction with a parameter $\delta_{ei}=\delta$ fixed to $\delta=0.2a$ or $\delta=0.4a$, where $a=(4\pi n/3)^{-1/3}$ is the Wigner-Seitz radius. For this kind of TCPs, the HNC method has already been extensively tested and evaluated by comparison of the resulting RDFs with those obtained by classical MD simulations [18]. For the numerical solution of the HNC scheme the dimensionless parameter $\sigma_{ei}=Ze_S^2 u_{ei}(0)/k_B T=\Gamma_{ei}(a/\delta)$—i.e., the maximum value of the electron-ion interaction energy in units of $k_B T$—plays an important role (see also Ref. [17,18]). Within our numerical treatment of the HNC equations a parameter regime with $\sigma_{ei}<\sigma_c(Z,\delta)$ is accessible, where the critical values σ_c for $\delta=0.1a$, $0.2a$, and $0.4a$ and the different studied TCPs (with ionic charge states $Z=1$, 3, 5, 7, 13, and 20) are given in Table I. Beyond this value the HNC numerical procedure does either not converge or ends up in unphysical solutions. A similar behavior has been reported in Ref. [17] for the case of an ion embedded in electrons. With the RDFs and $S_{\alpha\beta}(k)$ provided by the HNC scheme, the MFD $P(E)$ in the PMFEX+ model is then calculated via Eqs. (9) and (39)–(45) by standard numerical differentiation and integration methods [33]. In practice, it appears sufficient to terminate the sum in Eq. (43) at $l=5$.

TABLE I. Critical values $\sigma_c(Z,\delta)$ for some values of the ion charge Z and three values of $\delta=0.1a$, $0.2a$, and $0.4a$.

δ	$Z=1$	$Z=3$	$Z=5$	$Z=7$	$Z=13$	$Z=20$
$0.1a$	6.87	7.59	7.67	7.62	7.59	7.63
$0.2a$	6.55	7.68	7.52	7.13	6.66	6.48
$0.4a$	8.90	12.73	10.76	9.39	6.75	6.00

To test the PMFEX+ approximation and improvements compared to the standard PMFEX approach the calculated MFDs are confronted with those obtained by classical MD simulations. In the MD simulations the classical equations of motion are numerically integrated for N_i ions and $N_e=ZN_i$ electrons interacting via the regularized potentials $u_{\alpha\beta}(r)$. Such MD simulations have already been extensively tested and successfully applied for investigations of the dynamic properties [34–39] and the MFDs [18,19,40] of a TCP with regularized potentials and closely related problems [17] (see also Ref. [41] and references therein). In the numerical MD treatment all collisions and correlations in the simulated classical system are fully taken into account. Since both treatments—the numerical MD simulation and the theoretical model—are based on exactly the same underlying classical TCP with effective electron-ion interaction, the MD simulations thus provide reference data for approximative

treatments like the discussed PMFEX and PMFEX+ schemes. The only limitation of the MD simulations is the inevitable use of a finite simulation cube and periodic boundary conditions. This leads to some differences in the long-range contributions to the fields compared to theory (where infinite systems are considered), if the screening length is of the order or larger than the size of the simulation box. As the screening length gets shorter for increasing coupling or increasing ionic charge Z (at given n,T), this becomes relevant in particular for weak-coupling cases and may, at least in part, explain some of the deviations between theory and MD simulations which we observed in such cases (see below).

For the comparison envisaged we investigated two-component plasmas with different charge states $Z=1$, 3, 5, 7, 13, and 20 of the ions, corresponding to symmetric ($Z=1$) and highly asymmetric densities of the plasma species, and with certain values of the coupling parameters $\Gamma_{\alpha\beta}$ (with $\alpha,\beta=e,i$). At a given parameter δ, these coupling parameters $\Gamma_{\alpha\beta}$ are chosen to avoid the mentioned numerical difficulties with the HNC scheme and the formation of bound states in classical MD simulations. This implies in particular that for highly charged plasma ions with $Z\gg 1$ plasma states with strongly correlated ions ($\Gamma_{ii}\geqslant 1$) and strong electron-ion interactions ($\Gamma_{ei}\sim 1$) are accessible, while the parameter Γ_{ee} remains quite small, $\Gamma_{ee}\simeq\Gamma_{ei}/Z\ll 1$. But in the case of highly charged ions even for $\Gamma_{ee}\ll 1$ the electrons nevertheless may be strongly correlated due to nonlinear effects (see below). The MD simulations providing the present MFDs and RDFs have been performed using $N_{\mathrm{MD}}=N_i+N_e=5376$ particles. Further details on the applied MD technique can be found in Refs. [34–37]. As the theoretical models and the numerical solutions depend directly on the coupling parameters $\Gamma_{\alpha\beta}$ and the regularization parameter δ, we discuss, as, e.g., in Refs. [17–19], our results in terms of these parameters rather than in the underlying physical values of density and temperature.

Before discussing the MFD itself, we first consider briefly the RDFs and the validity of the HNC approximation for the parameters at hand. For small and moderate coupling where the parameter σ_{ei} is well below the critical value σ_c, the RDFs as either calculated by the HNC scheme or extracted from the MD simulations are always in perfect agreement (see, e.g., the corresponding examples given in Ref. [18]). Some typical examples for the RFDs at rather large coupling, where some deviations between HNC and MD may show up, are given in Figs. 1 and 2. Due to the regularization of the electron-ion interaction the RDF, $g_{ei}(r)$ is finite in the limit $r\to 0$ (not visible in Figs. 1 and 2) and can be approximated as $g_{ei}(0)\simeq\exp(\sigma_{ei}/\mathcal{R})$ with $\mathcal{R}=1+(\delta/a)(3\Gamma_{ei})^{1/2}$; see Refs. [17,18]. Thus the RDF $g_{ei}(r)$ shows the expected growth of correlations with increased coupling and decreased regularization parameter, where the HNC scheme tends to overestimate the value of $g_{ei}(0)$ (not visible in the figures). For example, for ions with charge state $Z=7$, $g_{ei}^{\mathrm{HNC}}(0)\simeq 57.4$, $g_{ei}^{\mathrm{MD}}(0)\simeq 48.8$ and $g_{ei}^{\mathrm{HNC}}(0)\simeq 107.3$, $g_{ei}^{\mathrm{MD}}(0)\simeq 96.4$ with $\delta=0.2a$, $\Gamma_{ee}=0.15$ and $\Gamma_{ee}=0.18$, respectively. At strong coupling deviations also occur in the electron-electron RDF $g_{ee}(r)$ at small r (as in the case of $Z=5$ and $Z=7$). The strong electron-ion interaction increases the electron density around the highly charged ion which introduces additional correlations between the electrons. This increases the probability of close electronic distances and results in the maxima in $g_{ee}(r)$ at distances $r\lesssim a$. This effect is obviously again overestimated in the HNC approach.

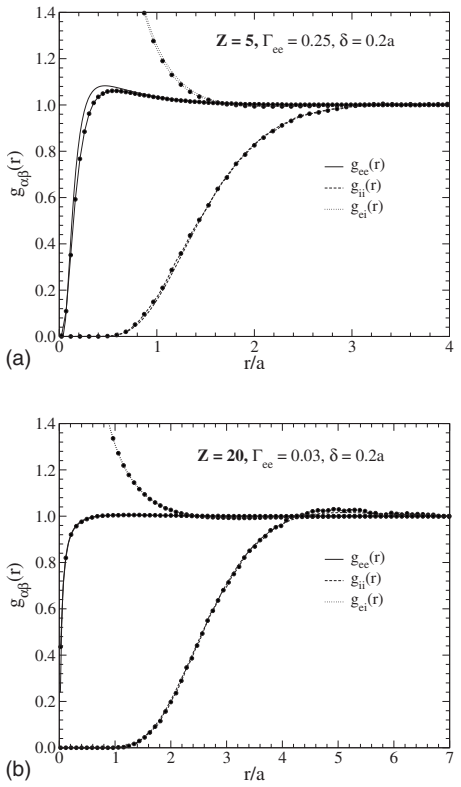

FIG. 1. RDFs $g_{\alpha\beta}(r)$ for plasmas with $\delta=0.2a$, $Z=5$, and $\Gamma_{ee}=0.25$ (a) and $Z=20$ and $\Gamma_{ee}=0.03$ (b). The lines correspond to the HNC approximation, while the symbols denote the MD simulations. The different lines represent g_{ee} (solid lines), g_{ii} (dashed lines), and g_{ei} (dotted lines).

In Figs. 3–8 we next compare the MFDs calculated from the PMFEX (dashed lines) and PMFEX+ (solid lines) schemes as well as from MD simulations (solid circles) where the electric microfields are scaled in units of the Holtsmark field E_H [see Eq. (3)]. In addition, the open circles are the Holtsmark MFDs for a TCP with Coulomb potential and the MFDs predicted by the first two terms of the standard BM series Eqs. (15)–(21) are shown as triangles. To demonstrate and test the proposed theoretical scheme we focus here on cases of strong coupling where the PMFEX and PMFEX+ results differ—i.e., where the higher-order corrections $\Delta\mathcal{L}(\kappa)$, Eq. (41), substantially contribute to the generating function $\mathcal{L}(\kappa)=\mathcal{L}_0(\kappa)+\Delta\mathcal{L}(\kappa)$. In all cases considered, however, the MFDs obtained both from the PMFEX and PMFEX+ treatments strongly differ from the standard BM electric field distributions and significantly improve the MFD at a neutral point compared to such weak-coupling approaches.

From the observed agreement with the MD simulations we found that the PMFEX+ scheme substantially improves the PMFEX model for TCPs with highly charged ions, whereas no clear improvement of the PMFEX+ method compared to the PMFEX can be seen in the case of a TCP

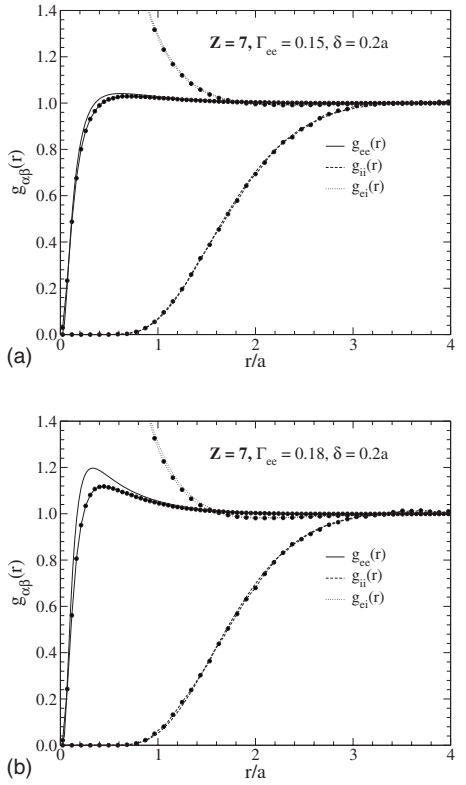

FIG. 2. Same as Fig. 1 for $Z=7$, $\delta=0.2a$, and $\Gamma_{ee}=0.15$ (a) and $\Gamma_{ee}=0.18$ (b).

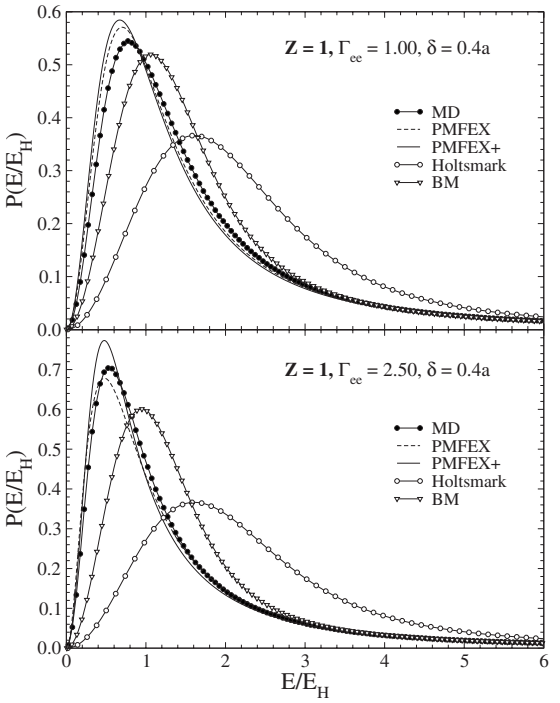

FIG. 3. Normalized electric microfield distributions for a plasma with $Z=1$, $\delta=0.4a$, $\Gamma_{ee}=\Gamma_{ii}=1$, and $\sigma_{ei}=3.15$ (top) and $\Gamma_{ee}=\Gamma_{ii}=2.5$ and $\sigma_{ei}=7.87$ (bottom) as a function of the electric field in units of E_H. The dashed and solid curves are the results of the PMFEX and PMFEX+ models, respectively. The solid circles represent the MFD from the MD simulations. The Holtsmark and standard Baranger-Mozer distributions are also shown as open circles and triangles, respectively.

with low ion charge. See the examples with $Z=1,3,5$, Figs. 3–5, compared to the obvious superiority of PMFEX+ in the examples with $Z>5$, Figs. 6–10. The deviations between theory and MD for low $Z\lesssim 5$ may be explained, at least in part, by the finite size of the simulation cube as outlined above. But this is needed together with a possible improvement of the theoretical model by adding higher orders of the further renormalized BM series investigations. We like to stress, however, that also for $Z\lesssim 5$ (Figs. 3–5) the PMFEX+ method yields a much better description of the MFD than the standard BM approach. And for ion charges $Z>5$, Figs. 6–8, the PMFEX+ predictions are in excellent agreement with the MD results [except for some smaller values of $P(E)$ near the maxima]. Here, the rather large deviation of the PMFEX method from the PMFEX+ method toward a higher probability of low fields (in particular in Figs. 6 and 8) indicates that the PMFEX method applied to the field at a neutral point does not correctly account for perturber-perturber correlations and, therefore, underestimates the MFDs at large fields. As expected for $Z_R=0$, all distributions shown in Figs. 3–8 merge at large electric fields, $\eta=E/E_H\gtrsim 6$, with the Holtsmark distribution with the asymptotic behavior $P_H(\eta)\simeq 1.496\eta^{-2.5}$. This indicates that due to electron-electron and ion-ion Coulomb interactions with $\delta_{ee}\simeq\delta_{ii}\simeq 0$, the second moments of the MFDs shown in Figs. 3–8 do not exist; see also Eq. (A7) derived in the Appendix.

To gain some more insight into the features and the range of validity of the PMFEX and PMFEX+ models we consider further increased coupling parameters as in Figs. 9 and 10. In the PMFEX scheme and for large values of Γ_{ee} the effective fields at large distances behave as $\mathcal{E}_\alpha(r)\sim\frac{1}{r}e^{-ar}\cos(br)$. Here a and b are some parameters increasing with Γ_{ee}, whereby the involved screening length a^{-1} does not necessarily coincide with the Debye length λ. The oscillatory nature of the effective fields drastically changes the properties of the generating function $\mathcal{L}_0(\kappa)$ in the PMFEX approximation [see Eq. (41)], which becomes negative at $\kappa E_H\gtrsim 1$. This is not the case in APEX approximation (as well as in the PMFEX approximation for a charged impurity ion—i.e., for the MFD at a charged point) where the effective field is treated in Debye-Hückel form and thus is positive and decreases monotoni-

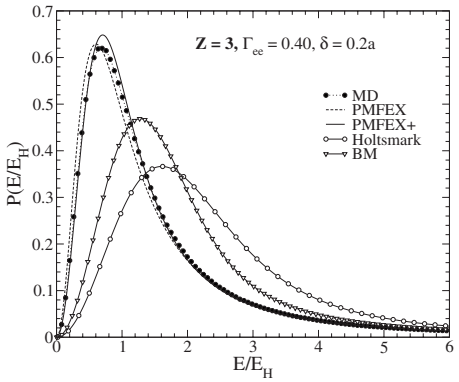

FIG. 4. Same as Fig. 3 for $Z=3$, $\Gamma_{ee}=0.4$, $\Gamma_{ii}=2.5$, $\sigma_{ei}=6.6$, and $\delta=0.2a$.

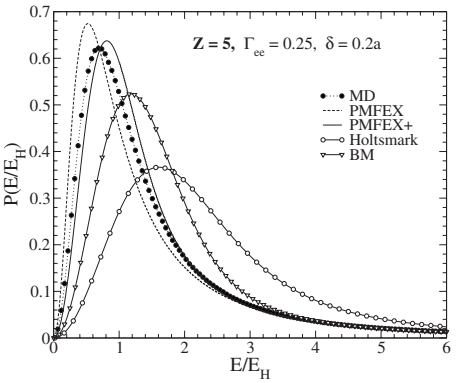

FIG. 5. Same as Fig. 3 for $Z=5$, $\Gamma_{ee}=0.25$, $\Gamma_{ii}=3.66$, $\sigma_{ei}=6.64$, and $\delta=0.2a$.

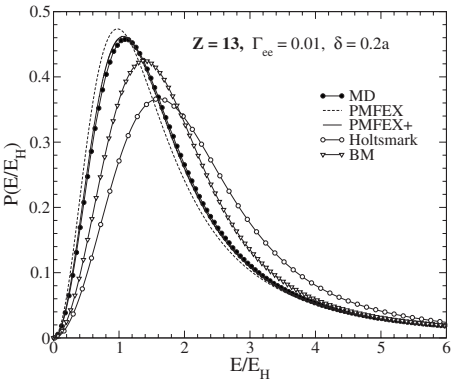

FIG. 7. Same as Fig. 3 for $Z=13$, $\Gamma_{ee}=0.01$, $\Gamma_{ii}=0.72$, $\sigma_{ei}=0.67$, and $\delta=0.2a$.

cally with r. Therefore the κ integration in Eq. (9) diverges and hence the PMFEX model becomes invalid for neutral radiators ($Z_R=0$) (and no curves for the PMFEX model can be given in Figs. 9 and 10). But even in this extreme regime the PMFEX+ model remains valid and the agreement with MD simulations is still quite good for the lower charge state $Z=7$ shown in Fig. 9 (although not as good as in Fig. 6) and almost perfect for the highly charged plasma ions ($Z=13,20$) as shown in Fig. 10.

As discussed above, some deviations between the HNC scheme and MD simulations occur in the electron-electron RDF $g_{ee}(r)$ at small distances $r \lesssim a$ for TCPs with $Z=5$ and $Z=7$; see the top panel of Fig. 1 and Fig. 2. Similarly the static structure factor $S_{ee}(k)$ obtained from the HNC scheme deviates from MD data at $ka \gtrsim 1$. This may be critical for the accuracy of the electronic effective field, Eq. (45), and hence for the generating function $\mathcal{L}(\kappa)$, Eqs. (39)–(41), calculated from the HNC approximation. Since the generating function is involved in the exponential factor $e^{-\mathcal{L}(\kappa)}$, even small deviations in $\mathcal{L}(\kappa)$ result in some appreciable deviations in the MFD. We therefore expect that the PMFEX+ predictions for the cases of $Z=5$ and $Z=7$ as presented in Figs. 5 and 9, respectively, will further improve if the MD data for the RDF $g_{ee}(r)$ is used as input.

VI. DISCUSSION AND CONCLUSION

In this paper we investigate the microfield distributions in a two-component plasmas with attractive electron-ion interactions. To this end we proposed in Ref. [18] the PMFEX model, which predicts the MFD very accurate in the case of a charged impurity ion, but requires further improvement for describing the MFD at a neutral point. It was thus our objective here to derive corrections to the PMFEX model by employing a renormalization of the standard Baranger-Mozer cluster expansion technique. For testing this amended theoretical scheme, denoted as PMFEX+, we focused on its capability to predict based on the HNC treatment of static correlations the MFD at a neutral point whereby MD simulations of the same underlying classical TCPs are providing the reference data. Here one of the basic assumptions is the regularization of the attractive electron-ion interaction at short distances to introduce quantum-diffraction effects in the employed classical approach. For the repulsive electron-electron and ion-ion interactions we assumed a bare Coulomb potential, for simplicity.

As examples, classical TCPs with ionic charge states $Z=1,3,5,7,13,20$ and hence with both symmetric and largely asymmetric densities of the plasma species were considered. Our treatment is limited to a parameter regime with $\sigma < \sigma_c$, where the critical values σ_c for $\delta=0.1a$, $0.2a$, and $0.4a$ are shown in Table I. Within this parameter regime the $g_{\alpha\beta}(r)$ from the HNC equations agree well with the MD simulations [except the correlation function $g_{ee}(r)$ for the cases given in Figs. 1 and 2]. At a further increase of the coupling and thus values of σ well beyond these critical σ_c the HNC equations

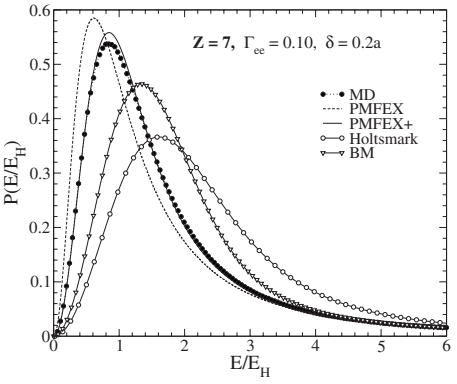

FIG. 6. Same as Fig. 3 for $Z=7$, $\Gamma_{ee}=0.1$, $\Gamma_{ii}=2.56$, $\sigma_{ei}=3.66$, and $\delta=0.2a$.

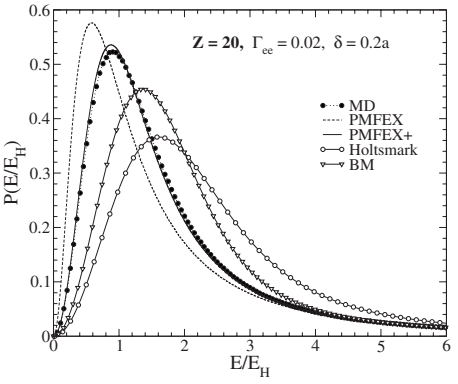

FIG. 8. Same as Fig. 3 for $Z=20$, $\Gamma_{ee}=0.02$, $\Gamma_{ii}=2.95$, $\sigma_{ei}=2.03$, and $\delta=0.2a$.

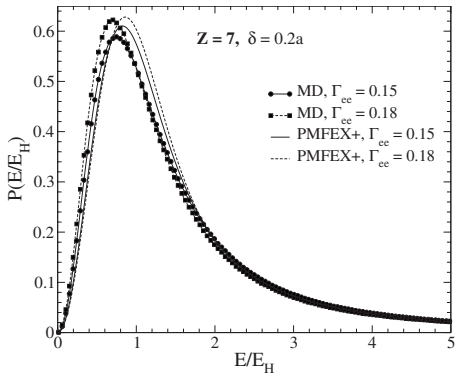

FIG. 9. Normalized electric microfield distributions for $Z=7$, $\Gamma_{ee}=0.15$ ($\Gamma_{ii}=3.85$, $\sigma_{ei}=5.49$), $\Gamma_{ee}=0.18$ ($\Gamma_{ii}=4.61$, $\sigma_{ei}=6.59$), and $\delta=0.2a$ as a function of the electric field in units of E_H. The solid and dashed curves are the results of the PMFEX+ model. The solid circles and squares represent the MFDs from the MD simulations.

either do not converge or end up in unphysical solutions. As we can deduce from our MD simulations, these are parameter regimes where a significant amount of bound states are formed in these classical systems.

For high charges of the plasma ions, $Z>5$, the PMFEX model is substantially improved by the new scheme and the agreement of the PMFEX+ model with the MD simulations is excellent, as shown in Figs. 6–8 and 10. For further increasing coupling the PMFEX scheme even becomes invalid

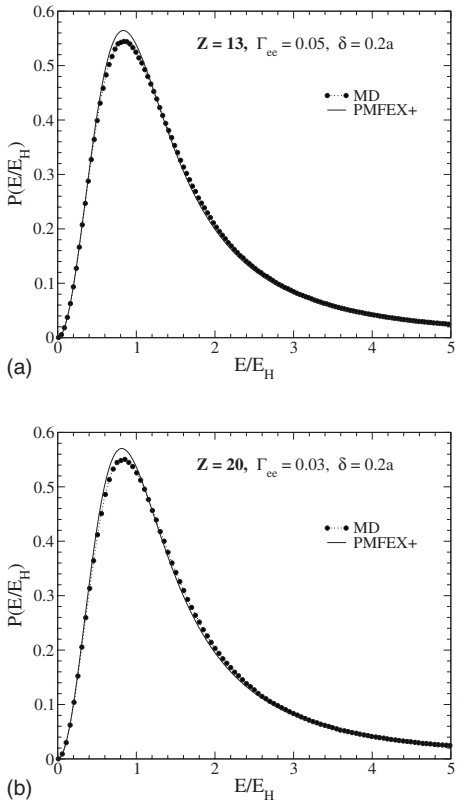

FIG. 10. Same as Fig. 9 for $Z=13$ (a) and $Z=20$ (b) with $\delta=0.2a$, $\Gamma_{ee}=0.05$, $\Gamma_{ii}=3.59$, $\sigma_{ei}=3.33$ and $\Gamma_{ee}=0.03$, $\Gamma_{ii}=4.42$, $\sigma_{ei}=3.05$, respectively.

while the PMFEX+ approach still works and yields good or almost perfect agreement with the MD; see Figs. 9 and 10. For a TCP with light ions—e.g., the case of $Z=3$, Fig. 4—the PMFEX and PMFEX+ approaches differ, but both somewhat deviate from the MD simulations as they do in the cases of $Z=1$, Fig. 3, and $Z=5$, Fig. 5. This regime of large coupling but moderate ionic charge state Z still needs some further investigation; probably, the renormalized Baranger-Mozer series should be truncated here at higher orders.

In summary, we note that the PMFEX approximation incorporates some key features of the MFD, in particular for large microfields E (small κ values). The large fields are predominantly due to configurations with a single-plasma particle near the position of the radiator. In this case the perturber-perturber correlations are less important and the PMFEX model as an independent-particle model is accurate for both neutral and charged radiators. The behavior of the MFD at large E is closely related to the behavior of the generating function $\mathcal{L}(\kappa)$ at small κ and how much accurate the exact second moment is involved in the model. At small κ the generating function behaves as $\mathcal{L}(\kappa)\simeq(\kappa^2/6)\langle E^2\rangle$ [see Eq. (12)], where the second moment $\langle E^2\rangle$ is exactly involved in the PMFEX model. Furthermore, the microfields in the large-field regime are asymptotically Gaussian distributed and characterized by the second moment $\langle E^2\rangle$. As discussed above, this is, however, not so for a neutral radiator and assuming bare Coulomb interactions between plasma particles where $\mathcal{L}(\kappa)$ behaves as $\sim\kappa^{3/2}$ at small κ and the MFDs are similar to the Holtsmark distribution at large E. Conversely, the small microfields (large κ values) are due to the additive effects of many particles at large distances and the PMFEX approximation is again accurate [18] except in the case of the neutral point where some deviations from MD simulations occur; see Figs. 3–8 and Ref. [19] for other examples. Therefore, the main uncertainty in the PMFEX model remains the domain of the intermediate configurations with $E\sim 1$ and $\kappa\sim 1$ (in units of E_H and $1/E_H$, respectively). Apparently, this domain is reduced by means of the renormalized (screened) fields $\mathcal{E}_\alpha(r)$ and the PMFEX model is much more adequate compared to the standard Baranger-Mozer (second-order) treatment. In the PMFEX+ model, on the other hand, imposing the renormalization procedure on the standard Baranger-Mozer series substantially improves their convergency, since $\psi_a^{(\alpha)}(\boldsymbol{\kappa})$ tends to zero for the relevant configurations more rapidly than $\chi_a^{(\alpha)}(\boldsymbol{\kappa})$. Finally, the PMFEX+ model may also be useful for a charged impurity ion in the cases where the PMFEX approximation deviates from MD. An example is the case of strongly coupled symmetric TCPs with $Z=1$ and a small regularization parameter δ as considered in Ref. [18].

For an application of the MFD obtained by the PMFEX and PMFEX+ schemes as the low-frequency contribution of the microfield in spectra modeling several further improvements would be desirable. In particular, for TCPs with high ion charges, the TCP should be replaced by a multicomponent plasma so that the actual charge-state distribution can be taken into account. This would result in a much more realistic description, which can be achieved by a corresponding straightforward extension of the PMFEX+ model together with the implementation and evaluation of the HNC scheme

for such a multicomponent plasma. Also the treatment of quantum effects is a source of further improvement in particular when dense plasmas at relative low temperatures are considered. Assuming that the connection between the RDFs $g_{\alpha\beta}$ and the MFD as established by the PMFEX and PMFEX+ models is (to some extent) also a reasonable approximation in the quantum case, the major task then consists in the calculation of the correlation functions $g_{\alpha\beta}$ by means of a full quantum description. Both items should thus be addressed in future studies of the MFD in strongly coupled plasmas.

An additional item for further investigations is the development of a theoretical model for the description of the MFD in case of a two-temperature (nonequilibrium) TCP. This is relevant in particular in the context of the spectroscopy of laser-generated plasmas, where usually the electrons are rapidly heated up first while the ions still remain at a rather low temperature. Assuming a transient quasistationary two-temperature regime the radial distribution functions can be calculated from HNC equations for a TCP with different ionic and electronic temperatures, as has already been done in Refs. [42,43]. There is, however, some additional theoretical effort needed, since the calculation of the MFD cannot be based on the canonical ensemble approach as in the outlined derivation of the PMFEX and PMFEX+ models. Here, a reasonable starting point might be the corresponding many-particle kinetic equations in connection with the potential-of-mean-force ansatz.

ACKNOWLEDGMENTS

This work was supported by the Bundesministerium für Bildung und Forschung (BMBF, 06ER145) and by the Gesellschaft für Schwerionenforschung (GSI, ER/TOE). The work of H.B.N. and D.A.O. has been partially supported by the Armenian Ministry of Higher Education and Science, Grants No. 0247 and No. 87. We gratefully acknowledge many stimulating discussions with C. Toepffer.

APPENDIX: EXACT SECOND MOMENT FOR A NEUTRAL RADIATOR

In this appendix we derive the exact second moment for the MFD in the TCP at the neutral point. We use the exact relation for the second moment derived in Ref. [18]:

$$\langle E^2\rangle = \frac{k_B T n_e}{Z_R \varepsilon_0}\left(\int_0^\infty \tilde{u}_e(r) g_{eR}(r) dr - \int_0^\infty \tilde{u}_i(r) g_{iR}(r) dr\right), \tag{A1}$$

where $\tilde{u}_\alpha(r) = -[r^2 u'_{\alpha R}(r)]'$ with $\alpha = e, i$ and the pair interaction potentials $u_{\alpha R}(r)$ are given by Eq. (4) with the regularization parameters $\delta_{\alpha R}$.

The second moment $\langle E^2\rangle$ is ill defined for the neutral-point distribution since $Z_R \to 0$ and $g_{\alpha R}(r) \to 1$ and the expression in brackets in Eq. (A1) vanishes in this case (this is true for the Coulomb potential as well as for any potential regularized at the origin). To obtain the correct limit of Eq. (A1) at $Z_R \to 0$ we recall the definition of the correlation functions $g_{\alpha R}(r)$ [18]. At vanishing Z_R this function reads

$$g_{\alpha R}(r) - 1 = -\frac{Z_R e_S^2}{k_B T}\left\{ q_\alpha u_{\alpha R}(r) + \sum_\beta q_\beta n_\beta \int d\mathbf{r}_1 u_{\beta R}(r_1) \times [g_{\alpha\beta}(|\mathbf{r} - \mathbf{r}_1|) - 1] \right\} + O(Z_R^2). \tag{A2}$$

Here $g_{\alpha\beta}(r)$ are the equilibrium correlation functions. Note that the second term on the right-hand side of Eq. (A2) is the excess potential energy of the TCP. In particular, using Eq. (A2) it is straightforward to calculate the effective field $\mathcal{E}_\alpha(r)$ for the neutral point. Insertion of this relation into Eq. (28) in the limit $Z_R \to 0$ and for Coulomb electron-electron and ion-ion interactions yields Eq. (27) with $g_{\alpha R}(r) = 1$ [see also Eq. (45)].

Now we substitute Eq. (A2) into Eq. (A1). In the limit of vanishing charge, $Z_R \to 0$ this yields

$$\langle E^2\rangle = 4\pi \sum_\alpha n_\alpha \int_0^\infty E_\alpha^2(r) r^2 dr + 16\pi^2 n_e^2 e_F^2 \times \left\{ \sum_\alpha \int_0^\infty [g_{\alpha\alpha}(r) - 1] \Psi_{\alpha\alpha}(r) r\, dr - 2\int_0^\infty [g_{ei}(r) - 1] \Psi_{ei}(r) r\, dr \right\}, \tag{A3}$$

where $E_\alpha(r) = -q_\alpha e_F u'_{\alpha R}(r)$ is the single-particle electric field with $q_e = -1$ and $q_i = Z$, $U_\beta(r) = [r u_{\beta R}(r)]'$, and

$$\Psi_{\alpha\beta}(r) = \frac{1}{2}\int_0^\infty [U_\beta(|\rho - r|) - U_\beta(\rho + r)] u_{\alpha R}(\rho) \rho\, d\rho. \tag{A4}$$

The first term in Eq. (A3) is the averaged density of the electric microfield energy (self-energy); the second one is the density of the excess electric energy which appears due to the correlations between plasma particles. Assuming a regularized interaction potential (4), we obtain $U_\beta(r) = e^{-r/\delta_{\beta R}}/\delta_{\beta R}$ and

$$\Psi_{ei}(r) = 1 - \frac{1}{2} e^{-r/\delta_{iR}} - \frac{e^{-r/\delta_{eR}} - e^{-r/\delta_{iR}}}{2(1-\Delta)} - \frac{e^{-r/\delta_{eR}} + \Delta e^{-r/\delta_{iR}}}{2(1+\Delta)}, \tag{A5}$$

$$\Psi_{\alpha\alpha}(r) = 1 - \left(1 + \frac{r}{2\delta_{\alpha R}}\right) e^{-r/\delta_{\alpha R}}. \tag{A6}$$

Here $\Delta = \delta_{iR}/\delta_{eR}$. In this case Eq. (A3) yields

$$\langle E^2\rangle = 2\pi n_e e_F^2 \left(\frac{1}{\delta_{eR}} + \frac{Z}{\delta_{iR}}\right) + 16\pi^2 n_e^2 e_F^2 \times \left\{ \sum_\alpha \int_0^\infty [g_{\alpha\alpha}(r) - 1] \Psi_{\alpha\alpha}(r) r\, dr - 2\int_0^\infty [g_{ei}(r) - 1] \Psi_{ei}(r) r\, dr \right\}, \tag{A7}$$

where $\Psi_{\alpha\alpha}(r)$ and $\Psi_{ei}(r)$ are now given by Eqs. (A5) and

(A6). The first term in Eq. (A7) is precisely the second moment of the Holtsmark distribution obtained in Ref. [18] for the regularized interactions, which is independent of Z_R. The second term arises due to correlations between particles. For the Coulomb interaction between plasma particles and the radiator with $\delta_{eR} \simeq 0$ or $\delta_{iR} \simeq 0$ the first term in Eq. (A7) diverges and the second moment of the MFD does not exist in this case.

[1] H. R. Griem, *Principles of Plasma Spectroscopy* (Cambridge University Press, Cambridge, England, 1997).
[2] D. Salzmann, *Atomic Physics in Hot Plasmas* (Oxford University Press, Oxford, 1998).
[3] J. Holtsmark, Ann. Phys. **58**, 577 (1919).
[4] J. E. Mayer and M. G. Mayer, *Statistical Mechanics* (Wiley, New York, 1940).
[5] M. Baranger and B. Mozer, Phys. Rev. **115**, 521 (1959).
[6] B. Mozer and M. Baranger, Phys. Rev. **118**, 626 (1960).
[7] C. F. Hooper, Jr., Phys. Rev. **149**, 77 (1966).
[8] C. F. Hooper, Jr., Phys. Rev. **165**, 215 (1968).
[9] C. A. Iglesias, J. L. Lebowitz, and D. MacGowan, Phys. Rev. A **28**, 1667 (1983).
[10] A. Alastuey, C. A. Iglesias, J. L. Lebowitz, and D. Levesque, Phys. Rev. A **30**, 2537 (1984).
[11] J. W. Dufty, D. B. Boercker, and C. A. Iglesias, Phys. Rev. A **31**, 1681 (1985).
[12] M. Yu. Romanovsky and W. Ebeling, Contrib. Plasma Phys. **46**, 195 (2006).
[13] U. Andiel *et al.*, Europhys. Lett. **60**, 861 (2002).
[14] See databases of bibliographic references on the Internet at http://physics.nist.gov/PhysRefData/Linebr/html/reffrm0.html [J. R. Fuhr, A. E. Kramida, H. R. Felrice, and K. Olsen (unpublished)].
[15] X.-Z. Yan and S. Ichimaru, Phys. Rev. A **34**, 2167 (1986).
[16] J. Ortner, I. Valuev, and W. Ebeling, Contrib. Plasma Phys. **40**, 555 (2000).
[17] B. Talin, A. Calisti, and J. Dufty, Phys. Rev. E **65**, 056406 (2002); B. Talin and J. Dufty, Contrib. Plasma Phys. **41**, 195 (2001); B. Talin, A. Calisti, J. W. Dufty, and I. V. Pogorelov, Phys. Rev. E **77**, 036410 (2008)
[18] H. B. Nersisyan, C. Toepffer, and G. Zwicknagel, Phys. Rev. E **72**, 036403 (2005).
[19] H. B. Nersisyan and G. Zwicknagel, J. Phys. A **39**, 4677 (2006).
[20] T. Morita, Prog. Theor. Phys. **22**, 757 (1959); **23**, 1211 (1960).
[21] G. Kelbg, Ann. Phys. **12**, 219 (1963); **13**, 354 (1964); **14**, 394 (1964).
[22] C. Deutsch, Y. Furutani, and M. M. Gombert, Phys. Rep. **69**, 85 (1981); C. Deutsch, Phys. Lett. **60A**, 317 (1977); C. Deutsch, M.-M. Gombert, and H. Minoo, *ibid.* **66A**, 381 (1978); H. Minoo, M.-M. Gombert, and C. Deutsch, Phys. Rev. A **23**, 924 (1981).
[23] A. Munster, *Statistical Thermodynamics* (Springer, Berlin, 1969), Vol. 1, Appendix 7.
[24] B. Held and C. Deutsch, Phys. Rev. A **24**, 540 (1981).
[25] A. Davletov and M.-M. Gombert, Phys. Rev. E **70**, 046404 (2004).
[26] C. de Dominicis and P. Martin, J. Math. Phys. **5**, 14 (1964).
[27] C. A. Iglesias and J. L. Lebowitz, Phys. Rev. A **30**, 2001 (1984); C. A. Iglesias, H. E. DeWitt, J. L. Lebowitz, D. MacGowan, and W. B. Hubbard, *ibid.* **31**, 1698 (1985).
[28] J.-P. Hansen and I. R. McDonald, *Theory of Simple Liquids* (Academic, New York, 1976).
[29] M. Baus and J. P. Hansen, Phys. Rep. **59**, 1 (1980).
[30] R. W. Zwanzig, J. Chem. Phys. **22**, 1420 (1954).
[31] I. S. Gradshteyn and I. M. Ryzhik, *Table of Integrals, Series and Products* (Academic, New York, 1980).
[32] T. Reed and K. Gubbins, *Applied Statistical Mechanics* (McGraw-Hill, New York, 1973).
[33] W. H. Press, B. P. Flannery, S. A. Teukolsky, and W. T. Vetterling, *Numerical Recipes* (Cambridge University Press, Cambridge, England, 1989).
[34] T. Pschiwul and G. Zwicknagel, Contrib. Plasma Phys. **41**, 271 (2001).
[35] A. Selchow, G. Röpke, A. Wierling, H. Reinholz, T. Pschiwul, and G. Zwicknagel, Phys. Rev. E **64**, 056410 (2001).
[36] T. Pschiwul and G. Zwicknagel, J. Phys. A **36**, 6251 (2003).
[37] G. Zwicknagel and T. Pschiwul, Contrib. Plasma Phys. **43**, 393 (2003).
[38] I. Morozov, H. Reinholz, G. Röpke, A. Wierling, and G. Zwicknagel, Phys. Rev. E **71**, 066408 (2005).
[39] G. Zwicknagel and T. Pschiwul, J. Phys. A **39**, 4359 (2006).
[40] J. Marten and C. Toepffer, Eur. Phys. J. D **29**, 397 (2004).
[41] A. Calisti, T. del Río Gaztelurrutia, and B. Talin, High Energy Density Phys. **3**, 52 (2007).
[42] P. Seuferling, J. Vogel, and C. Toepffer, Phys. Rev. A **40**, 323 (1989).
[43] V. Schwarz, Th. Bornath, W. D. Kraeft, S. Glenzer, A. Höll, and R. Redmer, Contrib. Plasma Phys. **47**, 324 (2007).